2013 IEEE International Conference on Robotics and Automation (ICRA)
Karlsruhe, Germany, May 6-10, 2013

# Constrained Motion Control of Multisegment Continuum Robots for Transurethral Bladder Resection and Surveillance

Andrea Bajo, Ryan B. Pickens, S. Duke. Herrell, and Nabil Simaan

***Abstract*—Constrained motion control of robotic end-effectors is essential for safe operation in confined spaces such as the urinary bladder. This paper presents the clinical motivation for the development of new control algorithms for robotic-assisted transurethral bladder resection and surveillance using multisegment continuum robots. The anatomy, workspace, and access constraints for this procedure are identified and used as a guideline for the design of the telesurgical system and its control architecture. Constraints are mapped into the configuration space of the robot rather than in task space simplifying the modeling and the enforcement of virtual fixtures. The redundancy resolution is autonomously modified in order to exploit the remaining degrees of freedom using task priority. These methods are validated on a glass model of urinary bladder.**

## I. Introduction

Continuum robots [1] are continuously bending, infinite degree-of-freedom flexible structures that provide intrinsic safety and increased intracorporeal dexterity. In the past ten years, researchers have investigated continuum robots for several surgical applications such as transoral throat surgery [2], cardiac surgery [3], [4], skull base surgery [5], and transurethral resection [6]. Whether it is a laryngoscope, a trocar, a vein, the nasal cavity, or the urethra (see Fig. 1), soft and hard constraints confine the motion of these robots at multiple points along their structures.

As continuum robots reach deeper surgical sites, sensory presence, trajectory planning, and the enforcement of virtual fixtures is crucial for completing complex surgical tasks such as navigation in unstructured environments, suturing, knot tying, and dissection. In [7], [8], the authors investigated obstacle avoidance for hyper-redundant robots using geometric methods. In [9], [10], the authors proposed a library of virtual fixtures for key surgical tasks. In [11], the authors investigated path planning of steerable needles. These methods focus on the end-effector by either solving an optimization problem during path planning or enforcing task-space virtual fixtures. In this paper we propose to enforce virtual fixtures in the configuration space rather than task space and automatically adjusts the redundancy resolution for optimal tracking during constrained motion.

The motivation behind this work stems from the challenges of transurethral resection of bladder tumor (TURBT). Recent works have mainly focused on adaptation of commercially available devices. For example, a master-slave system for controlling a commercial resectoscope is described in [12], an adaptation of a commercial robotic catheter system is discussed in [13], a slave manipulator for transurethral prostate resection was proposed in [14], and a shape memory alloy actuated mechanism was presented in [15]. More recently, a telerobotic platform for both intervention and surveillance was proposed in [6]. This system was designed to improve and expand the repertoire of techniques of urologic surgery, to increase surgical resection accuracy, and surveillance coverage. However, in order to reach the anterior and interior quadrants of the urinary bladder (Fig. 1), the continuum robot (Fig. 2) needs to safely and autonomously retract inside the resectoscope allowing localized constrained telemanipulation of its end-effector.

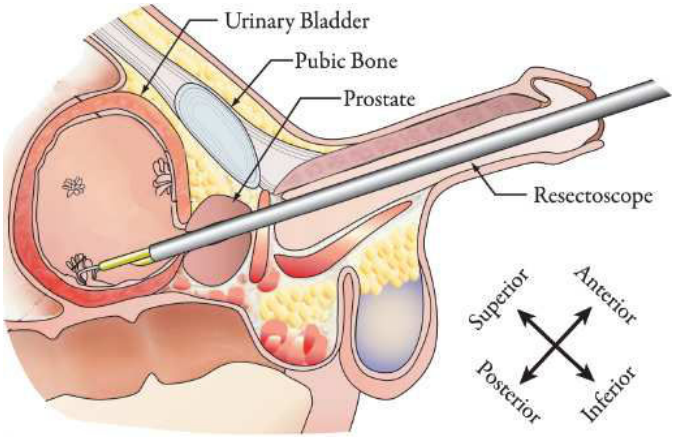


Fig. 1. Overview of transurethral intervention and surveillance. The instruments access the urinary bladder through the resectoscope, a long, tubular, channel.

The contribution of this paper is in proposing the enforcement of virtual fixtures in the configuration space of the manipulator rather than in the task space as previously proposed in literature (i.e. [16]). In the case of continuum robots, the burden of safeguarding both the anatomy and the surgical slave can not be left to the surgeon. On the other hand, intelligent surgical slaves should be able to autonomously steer away from access and anatomical constraints and adjust the inversion of the kinematics. The configuration space often provides a lower-order space in which constraints along subsequent segments can be easily and intuitively defined. The framework is evaluated on a 5 DoF continuum robot for transurethral intervention. Experimental results show the ability to cover 100% of the urinary bladder.

This work was supported by Vanderbilt University internal funds. A. Bajo and N. Simaan were also supported by NSF Career grant No. IIS-1063750

A. Bajo and N. Simaan are with the Department of Mechanical Engineering, Vanderbilt University, Nashville, TN 37212, USA.

R. B. Pickens and S. D. Herrell are with the Department of Urology, Vanderbilt University Medical Center, Nashville, TN 37212, USA.

Fig. 2. The telesurgical system for bladder resection and surveillance in an explanted bovine bladder.

## II. Clinical Motivation

TURBT is an endoscopic surgical procedure that aims for resecting non-invasive tumors inside the urinary bladder. In 2012, the number of newly diagnosed bladder cancer patients and deaths in the US are expected to be 73,510 and 14,880 respectively [17]. TURBT procedures provide access to the bladder via the urologic resectoscope, a device that consists of multiple telescoping and interlocking parts. The inner diameter that is used to deliver instruments and visualization is typically between 7 and 8 mm. The resectoscope is inserted through the urethra as shown in Fig. 1.

The long straight access channel reduces dexterity at the tool tip by only allowing insertion along the resectoscope's axis and limiting lateral movements that are usually achieved by re-orienting the resectoscope and the surrounding anatomy. Coverage of the posterior and superior quadrant is difficult and accuracy of the resection highly depends on surgeon skills. Coverage of the anterior and inferior quadrant is achieved by pushing on the pubic bone in order to deform the urinary bladder internal wall.

In order to address these challenges, in [6], we proposed the telesurgical system of Fig. 2 and evaluated deployment, laser delivery, and biopsy inside an explanted bovine bladder. Posterior and superior quadrants of the urinary bladder were easily reached and key surgical tasks were performed. On the other hand, the anterior and inferior quadrants were not easily accessed under telemanipulation control because of the inability of the operator to safely retract the continuum arm inside the resectoscope and accomplish the desired movement with the deployed portion of the manipulator. In order to perform any surgical procedure in these areas of the bladder, the surgical slave should actively assist the surgeon by avoiding the tubular constraint without *a priori* knowledge of the task while allowing full control of the remaining DoF. Traditional virtual fixture methods that constraint the robot's end-effector may not easily exploited in this scenario because of the fact that the virtual fixtures need to be applied to section of the manipulator only (in this case the first segment). Furthermore, these virtual fixtures do not only depend on the particular access channel used but only on the insertion depth along the tubular constraint.

## III. Constrained kinematics and configuration space virtual fixtures

The surgical slave of Fig. 3 is the composition of a linear stage and a dexterous four DoF continuum manipulator. Each segment has three *push-pull* backbones that allows for bending in space. A complete derivation of the direct and differential kinematics of these continuum structures are given in [2]. For the ease of presentation, in the remainder of this section, the kinematics of the two segments and the insertion stage is summarized.

### A. Direct Kinematics

The direct kinematics of the surgical slave is depicted in Fig. 3. Five coordinate systems are defined: 1) base frame $\{\hat{\mathbf{x}}_0, \hat{\mathbf{y}}_0, \hat{\mathbf{z}}_0\}$, 2) first segment base disk frame $\{\hat{\mathbf{x}}_1, \hat{\mathbf{y}}_1, \hat{\mathbf{z}}_1\}$, 3) second segment base disk frame $\{\hat{\mathbf{x}}_2, \hat{\mathbf{y}}_2, \hat{\mathbf{z}}_2\}$, 4) end-effector frame $\{\hat{\mathbf{x}}_3, \hat{\mathbf{y}}_3, \hat{\mathbf{z}}_3\}$, and 5) tool frame $\{\hat{\mathbf{x}}_4, \hat{\mathbf{y}}_4, \hat{\mathbf{z}}_4\}$. The position and the orientation of the end-effector in base frame is given by:

$$\mathbf{p}_3^0 = \mathbf{p}_1^0 + \mathbf{R}_1^0 \left(\mathbf{p}_2^1 + \mathbf{R}_2^1 \mathbf{p}_3^2\right) \tag{1}$$

$$\mathbf{R}_3^0 = \mathbf{R}_1^0 \mathbf{R}_2^1 \mathbf{R}_2^3. \tag{2}$$

where $\mathbf{p}_1^0$ is given by the amount of insertion/retraction (see Fig 3

$$\mathbf{p}_1^0 = \begin{bmatrix} 0 & 0 & q_{ins} \end{bmatrix}^T, \tag{3}$$

and the position of the end disk of each segment ($k = 1, 2$) is given by

$$\mathbf{p}_{k+1}^k = \frac{L_k}{\theta_k - \theta_0} \begin{bmatrix} \cos(\delta_k)\left(\sin(\theta_k) - 1\right) \\ -\sin(\delta_k)\left(\sin(\theta_k) - 1\right) \\ -\cos(\theta_k) \end{bmatrix} \quad k = 1, 2. \tag{4}$$

where $L_k$ is the length of segment $k$, $\theta_k$ is the bending angle, $\delta_k$ defines the angle in which segment $k$ bends, $q_{ins}$ is the displacement of frame $\{1\}$ from frame $\{0\}$ along $\hat{\mathbf{z}}_0$, $\theta_0 = \pi/2$, $\mathbf{R}_1^0$ is the identity matrix (see [2] for a design in which the first segment base disk rotates),

$$\mathbf{R}_{k+1}^k = Rot\left(-\delta_k, \hat{\mathbf{z}}\right) Rot\left(\theta_0 - \theta_k, \hat{\mathbf{y}}\right) Rot\left(\delta_k, \hat{\mathbf{z}}\right) \tag{5}$$

and operator $Rot(\phi, \hat{\mathbf{w}})$ returns a rotation of angle $\phi$ about axis $\hat{\mathbf{w}}$. The direct kinematics of the surgical slave is easily updated if a tool is deployed through one of its access channels. In this case, the position of the tools is given by:

$$\mathbf{p}_4^0 = \mathbf{p}_3^0 + \mathbf{R}_3^0 \begin{bmatrix} r_c \cos\beta & r_c \sin\beta & d_3 \end{bmatrix}^T \tag{6}$$

We now define the configuration space $\Psi \in \mathbb{R}^5$ and the joint space $\mathbf{q} \in \mathbb{R}^7$. The configuration space is defined as:

$$\Psi = \begin{bmatrix} \theta_1 & \delta_1 & \theta_2 & \delta_2 & q_{ins} \end{bmatrix}^T \tag{7}$$

while the joint space is defined as:

$$\mathbf{q} = \begin{bmatrix} q_{1,1} & q_{1,2} & q_{1,3} & q_{2,1} & q_{2,2} & q_{2,3} & q_{ins} \end{bmatrix}^T \tag{8}$$

where, for segments $k = 1, 2$ and backbones $i = 1, 2, 3$:

$$q_{k,i} = r \cos\left(\delta_k + i\beta\right)\left(\theta_i - \theta_0\right). \tag{9}$$

### B. Differential Kinematics

The end-effector translational and rotational velocities are obtained as:

$$\mathbf{v}^0_{0,3} = \mathbf{v}^0_{0,1} + \mathbf{R}^0_1\left(\mathbf{v}^1_{1,2} + \mathbf{R}^1_2\mathbf{v}^2_{2,3} + \omega^1_{1,2}\times\mathbf{R}^1_2\mathbf{p}^2_3\right) \quad (10)$$

$$\omega^0_{0,3} = \mathbf{R}^0_1\omega^1_{1,2} + \mathbf{R}^0_2\omega^2_{2,3} \quad (11)$$

where $\mathbf{v}^c_{a,b}$ and $\omega^c_{a,b}$ are the translational and rotational velocities of frame $b$ with respect to frame $a$ written in frame $c$. The translational velocity of frame $\{1\}$, $\mathbf{v}^0_{0,1}$, is give by differentiating (3) with respect to time while the translational velocities of the first, $\mathbf{v}^1_{1,2}$, and second end disk, $\mathbf{v}^2_{2,3}$, in local coordinate frames is given by differentiating (4) with respect to time for $k = 1, 2$. Rotational velocity $\omega^1_{1,2}$ and $\omega^2_{2,3}$ are given by (for $k = 1, 2$):

$$\omega^{k-1}_{k-1,k} = \dot{\theta}_k\hat{\mathbf{y}}^{k-1}_k + \dot{\delta}_k\left(\hat{\mathbf{z}}^{k-1}_k - \hat{\mathbf{z}}^{k-1}_{k-1}\right). \quad (12)$$

By defining $\dot{\Psi}$ as the rate of change of the configuration space vector $\Psi$, one can rewrite the twist of the end-effector (i.e. (10) and (11)) as:

$$\begin{bmatrix} \mathbf{v}^0_{0,3} \\ \omega^0_{0,3} \end{bmatrix} = \mathbf{J}_{arm}\dot{\Psi}. \quad (13)$$

The geometric Jacobian $\mathbf{J}_{arm}$ is the result of three contributions: the insertion linear stage, and the two continuum segments:

$$\mathbf{J}_{arm} = \begin{bmatrix} \mathbf{S}_1\mathbf{J}_1 & \mathbf{S}_2\mathbf{J}_2 & \mathbf{e}_3 \end{bmatrix} \quad (14)$$

where $\mathbf{e}_3 = \begin{bmatrix} 0 & 0 & 1 & 0 & 0 & 0 \end{bmatrix}^T$. Assuming circular bending [18], each continuum segment Jacobian $k = 1, 2$ is then given by [19]:

$$\mathbf{J}_k = \begin{bmatrix} L_k c_{\delta_k}\frac{\Theta_k c_{\theta_k} - s_{\theta_k} + 1}{\Theta_k^2} & -\frac{L_k s_{\delta_k}\left(s_{\theta_k}-1\right)}{\Theta_k} \\ -L_k s_{\delta_k}\frac{\Theta_k c_{\theta_k} - s_{\theta_k} + 1}{\Theta_k^2} & -\frac{L_k c_{\delta_k}\left(s_{\theta_k}-1\right)}{\Theta_k} \\ L_k\frac{\Theta_k s_{\theta_k} + c_{\theta_k}}{\Theta_k^2} & 0 \\ -s_{\delta_k} & c_{\delta_k}c_{\theta_k} \\ -c_{\delta_k} & -s_{\delta_k}c_{\theta_k} \\ 0 & -1 + s_{\theta_k} \end{bmatrix} \quad (15)$$

where $c_y = \cos(y)$, $s_y = \sin(y)$, and transformation matrices $\mathbf{S}_1$ and $\mathbf{S}_2$ are given by:

$$\mathbf{S}_1 = \begin{bmatrix} \mathbf{I} & \left[-{}^0\mathbf{R}_2\,{}^2\mathbf{p}_3\right]\times \\ \mathbf{0} & \mathbf{I} \end{bmatrix} \quad (16)$$

$$\mathbf{S}_2 = \begin{bmatrix} {}^0\mathbf{R}_2 & \mathbf{0} \\ \mathbf{0} & {}^0\mathbf{R}_2 \end{bmatrix}. \quad (17)$$

### C. Constrained Redundancy Resolution

The surgical slave is teleoperated using a Sensable Phantom Omni and the master/slave trajectory planner presented in [20]. Once the desired twist of the slave's end-effector, $\mathbf{t}_{des}$, is obtained, the constrained configuration space velocities, $\dot{\mathbf{\Psi}}_{des}$, that approximate the desired motion are computed. As described in Section III-A, the surgical slave is only capable to control 3 translational DoFs and two rotational DoFs (point in space). Furthermore, when the first segment is retracted inside the tubular constraint, the controllable DoFs drops to 3 (2 rotational DoFs and insertion along the resectoscope). For these reasons, we defined a primary task and secondary task. The primary task consists of controlling the two rotational DoFs (rotations about $\hat{\mathbf{x}}_0$ and $\hat{\mathbf{y}}_0$) and one translational DoF (along $\hat{\mathbf{z}}_0$) while the secondary task consists of controlling the remaining two translational DoF (along $\hat{\mathbf{x}}_0$ and $\hat{\mathbf{y}}_0$).

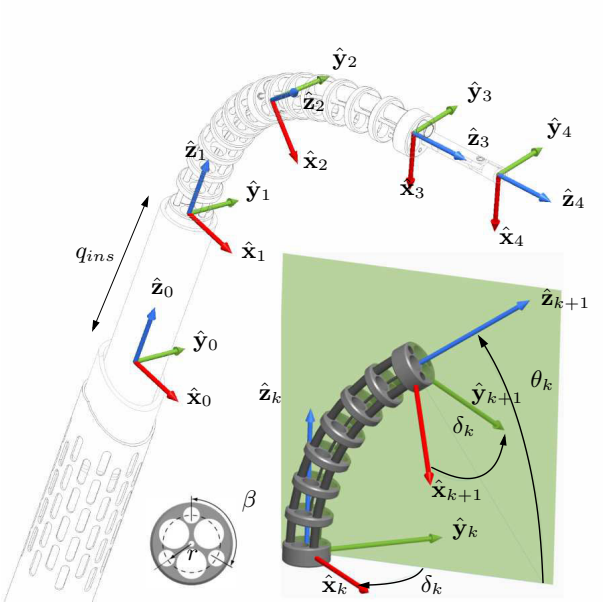


Fig. 3. Kinematics nomenclature of the surgical system. Angle $\delta_k$ defines the plane in which the continuum segment bends while $\theta_k$ designates the bending angle.

Designating $\mathbf{t}_{ee}$ and $\mathbf{J}_{ee}$ as the end effector twist and Jacobian in end-effector frame, one may describe the primary and secondary tasks by:

$$\mathbf{J}_{S_p}\dot{\mathbf{\Psi}}_{des} = \mathbf{S}_p\mathbf{t}_{ee}, \quad \mathbf{J}_{S_s}\dot{\mathbf{\Psi}}_{des} = \mathbf{S}_s\mathbf{t}_{ee} \quad (18)$$

where $\mathbf{J}_{S_p}$ and $\mathbf{J}_{S_s}$ are defined by selecting the corresponding task-specific rows of the jacobian:

$$\mathbf{J}_{S_p} = \mathbf{S_p}\mathbf{J}_{ee}, \quad \mathbf{J}_{S_s} = \mathbf{S_s}\mathbf{J}_{ee} \quad (19)$$

and selection matrices $\mathbf{S}_p$ and $\mathbf{S}_s$ are given by:

$$\mathbf{S}_p = \begin{bmatrix} 0&0&1&0&0 \\ 0&0&0&1&0 \\ 0&0&0&0&1 \end{bmatrix}, \quad \mathbf{S}_s = \begin{bmatrix} 1&0&0&0&0 \\ 0&1&0&0&0 \end{bmatrix} \quad (20)$$

The end effector twist and Jacobian are given by:

$$\mathbf{J}_{ee} = \begin{bmatrix} \mathbf{I}_{5\times5} & \mathbf{0}_{5\times1} \end{bmatrix}\begin{bmatrix} \mathbf{R}^{0T}_3 & \mathbf{0}_{3\times3} \\ \mathbf{0}_{3\times3} & \mathbf{R}^{0}_3T \end{bmatrix}\mathbf{J}_{arm} \quad (21)$$

$$\mathbf{t}_{ee} = \begin{bmatrix} \mathbf{I}_{5\times5} & \mathbf{0}_{5\times1} \end{bmatrix}\begin{bmatrix} \mathbf{R}^{0T}_3 & \mathbf{0}_{3\times3} \\ \mathbf{0}_{3\times3} & \mathbf{R}^{0T}_3 \end{bmatrix}\mathbf{t}_{des}. \quad (22)$$

The desired configuration space velocity is therefore given by:

$$\dot{\Psi}_{des} = \left(\mathbf{J}^{\dagger}_{S_p}\mathbf{S}_p + \left(\mathbf{I} - \mathbf{J}^{\dagger}_{S_p}\mathbf{J}^T_{S_p}\right)\mathbf{J}^{\dagger}_{S_s}\mathbf{S_s}\right)\mathbf{t}_{ee} \quad (23)$$

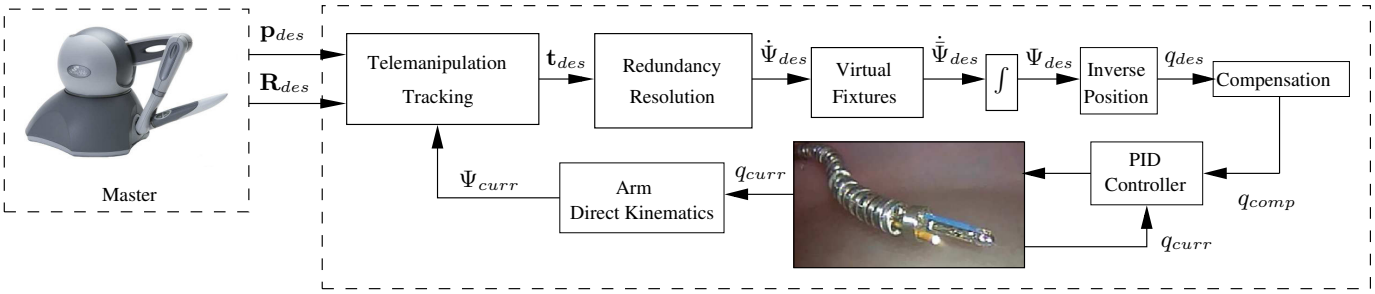


Fig. 4. Control architecture of the surgical robotic system.

and superscript † indicates pseudo-inverse. Equation (23) partitions the commanded twist, $\mathbf{t}_{ee}$, into a primary task (defined by selection matrix $\mathbf{S}_p$) and a secondary task (defined by selection matrix $\mathbf{S}_s$). Equations (21) and (22) are respectively the Jacobian matrix and the end-effector twist expressed in end-effector frame without the angular velocity component about axis $\hat{\mathbf{z}}_3$. By doing so, any commanded twist about that axis is ignored by the redundancy resolution and the continuum manipulator is controlled in 5 DoF.

### D. Virtual Fixture Design and Implementation

We now define two orthogonal spaces that partition the configuration space into a subspace of forbidden velocities $\{\bar{V}\}$ and a space of allowed velocities $\{V\}$. We can therefore two projection matrices that project the configuration space velocities of 23 into forbidden and allowed velocities:

$$\bar{\mathbf{P}} = \bar{\mathbf{V}}(\bar{\mathbf{V}}^T\bar{\mathbf{V}})^{\dagger}\bar{\mathbf{V}}^T \tag{24}$$

$$\mathbf{P} = \mathbf{I} - \bar{\mathbf{P}} \tag{25}$$

where † denotes pseudo-inverse for the case where $\bar{V}$ is (column) rank deficient. For example, in the case of a tubular constraint, as the first segment of the continuum manipulator retracts inside the resectoscope, negative $\dot{\theta_1}$ is the forbidden configuration velocity and $\bar{\mathbf{V}}$ is defined as

$$\bar{\mathbf{V}} = \begin{bmatrix} 1 & 0 & 0 & 0 & 0 \end{bmatrix}^T. \tag{26}$$

The desired configuration space velocity is therefore given by:

$$\dot{\tilde{\Psi}}_{des} = \mathbf{P}\dot{\Psi}_{des} + k_d\bar{\mathbf{P}}\mathbf{u} \tag{27}$$

where $\mathbf{u} = f(\Psi)$ is a signed configuration space distance of the actual configuration $\Psi_{curr}$ to the one imposed by the virtual fixture $\Psi_{fix}$, and scalar $k_d$ determines how quickly the continuum manipulator is moved to the desired configuration. In the case of the surgical slave of Fig. 2, vector $\mathbf{u}$ and projection matrices $\bar{\mathbf{P}}$, $\mathbf{P}$ depend on the insertion variable $q$ along the resectoscope.

The desired configurations vector $\Psi_{des}$ is then obtained via *Resolved Motion Rate* [21]:

$$\Psi_{des} = \Psi_{curr} + \Delta_t\dot{\tilde{\Psi}}_{des} \tag{28}$$

Once the desired configuration vector is obtained, using the kinematics relationship presented in III-A one can compute the desired joint space position to be fed to the actuation compensation subsystem.

The application of virtual fixtures in the configuration space of the robot rather than in the operational space allows for easy correction of the motion of any portion of the continuum manipulator. The computation of projection matrices $\bar{\mathbf{P}}$, $\mathbf{P}$ and vector $\mathbf{u}$ is shown in Algorithm 1. As the robot is commanded to retract inside the resectoscope, the $\dot{\theta_1}$ direction is defined as forbidden and $\mathbf{u}$ depends on the following safe bending angle:

$$\theta_{1,safe} = \theta_{min} + (\theta_0 - \theta_{min})\frac{\|q_{ins}\|}{L_1}. \tag{29}$$

Figure 4 shows the complete control architecture of the surgical continuum robot. The desired pose is obtained from the master manipulator (Phantom Omni) at 125 Hz over the local area network. The telemanipulation tracking subsystem generates the desired task-space velocities according to the master-slave map as described in [20]. The redundancy resolution subsystem implements the algorithm described in section III-C while the virtual fixtures subsystems constructs and enforces the configuration space virtual fixtures as described in section III-D and Algorithm 1. Once the desired configuration space velocities are obtained, the desired joint-space positions are computed via the close-form inverse position analysis of the continuum manipulator and the model-based actuation compensation scheme of [22].

## IV. Experimental Results

### A. Experimental Setup

The experimental setup of Fig. 5 consists of a 7-axes actuation unit, a 2-segment ⌀5 mm continuum robot, a 250 ml beaker, and Sensable Phantom Omni (not shown). The beaker approximates an inflated average-sized urinary bladder. Target points on the outer surface of the beaker were marked for targeting experiments. This points are placed in the *interior* and *anterior* quadrants, the areas of the bladder that are not easily reached with conventional urologic instruments and the robot in normal telemanipulation mode.

### B. Constrained Targeting

In order to test the configuration space virtual fixtures and the constrained redundancy resolution presented in Section III, the robot was commanded to reach predetermined points inside the *interior* quadrant of the glass bladder. Points vary

**Algorithm 1** Virtual Fixture

**Input:** $\theta_1, \delta_1, \theta_2, \delta_2, q_{ins}$
**Input:** $\dot{\theta}_1, \dot{\delta}_1, \dot{\theta}_2, \dot{\delta}_2, \dot{q}_{ins}$
  **if** $q_{ins} \leq 0$ **then**
    $\bar{\mathbf{V}} \leftarrow \begin{bmatrix} \theta_1 & 0 & 0 & 0 & 0 \end{bmatrix}^T$
    $\bar{\mathbf{P}} \leftarrow \bar{V}(\bar{V}^T\bar{V})^{\dagger}\bar{V}^T$
    $\mathbf{P} \leftarrow \mathbf{I} - \bar{\mathbf{P}}$
    **if** $(\dot{q}_{ins} < 0)$ & $(\theta_1 \leq \theta_{min} + \theta_0\|q_{ins}\|/L_1)$ **then**
      $\mathbf{u} \leftarrow (\theta_{min} + \theta_0\|q_{ins}\|/L_1 - \theta_1) \begin{bmatrix} 1 & 0 & 0 & 0 & 0 \end{bmatrix}^T$
    **else**
      $\mathbf{u} \leftarrow \begin{bmatrix} 0 & 0 & 0 & 0 & 0 \end{bmatrix}^T$
    **end if**
  **else**
    $\bar{\mathbf{P}} = \mathbf{0}$
    $\mathbf{P} = \mathbf{I}$
    $\mathbf{u} \leftarrow \begin{bmatrix} 0 & 0 & 0 & 0 & 0 \end{bmatrix}^T$
  **end if**
  $\dot{\tilde{\Psi}}_{des} \leftarrow \mathbf{P}\dot{\Psi}_{des} + k_d\bar{\mathbf{P}}\mathbf{u}$
  **return** $\dot{\tilde{\Psi}}_{des}$

Fig. 5. The experimental setup consists of a 7-axes actuation unit, a urologic resectoscope, a 2-segment continuum robot, a 250 ml beaker, and three tubes with various diameters. The beaker approximates the size of an average-sized bladder when inflated while the tubes were used for testing targeting accuracy.

between configurations in which the robot is fully deployed inside the bladder (points close to the bladder *equator*) and points in which the continuum arm is partially inserted into the urologic resectoscope (points close to entry point). Fig. 6 and the Multimedia Extension show the continuum manipulator guided from one target point on the left of the interior quadrant to the right side of the interior quadrant in a partially deployed configuration. The picture sequence of Fig. 6 shows how the proximal segment (partially inserted into the resectoscope) automatically complies its motion to the tubular constraint while allowing the primary task to be accomplished. During the motion, the $\theta_1$ degree-of-freedom is autonomously adjusted in order not to violate the tubular constraint while the $\delta_1$ degree-of-freedom is freely exploited to accomplish the primary task.

### C. Constrained Targeting Accuracy

In order to evaluate constrained targeting accuracy, the operator was asked to insert a ⌀0.55 mm laser into a ⌀2.4 mm, ⌀1.62 mm, and ⌀0.9 mm tubes respectively. As shown in Multimedia Extension 2, the user was able to target all tubes. The clearance between the outer diameter of the laser fiber and inner diameter of the smallest tube gives a constrained targeting accuracy of better than 0.35 mm.

### D. Coverage

In order to evaluate the ability of the surgical slave to reach the whole urinary bladder additional telemanipulation experiments were conducted. The robot was deployed inside the glass bladder model and guided to *sweep* the posterior and the interior quadrants. A picture sequence is shown in Fig. 7. From left to right, each frame shows the continuum manipulator covering progressively the posterior and interior quadrant. The posterior quadrant is reached with the robot fully deployed and the insertion stage at its maximum insertion depth. In this case both segments are free to move in any direction and both primary and secondary tasks can be accomplished.

## V. Conclusions

TURBT procedures are fundamental for both diagnosis and treatment of bladder cancer. In this paper, we presented methods for constrained motion control of a novel surgical slave for TURBT. Virtual fixtures were designed in the configuration space of the robot manipulator rather than in task space and a multi-task constrained redundancy resolution was used to exploit the remaining DoFs. Experimental results demonstrated the efficacy of the proposed virtual fixture framework in targeting the interior and anterior walls of the bladder as well as the posterior and superior walls as previously demonstrated. These algorithms provide a step forward to intelligent surgical devices that are able to actively assist the surgeon by reducing some of the burden of safeguarding for anatomy, instruments, and the robotic manipulator. As continuum robots reach deeper inside the human anatomy and *become smarter* there is a need for ad-hoc master interfaces that exploit the full potential of these robots.

Fig. 6. Image sequence of constrained targeting in the interior quadrant (also contained in the Multimedia Extension). The first continuum segment is partially retracted inside the resectoscope. Its motion is autonomously limited by the configuration space virtual fixture while allowing for the completion of the task.

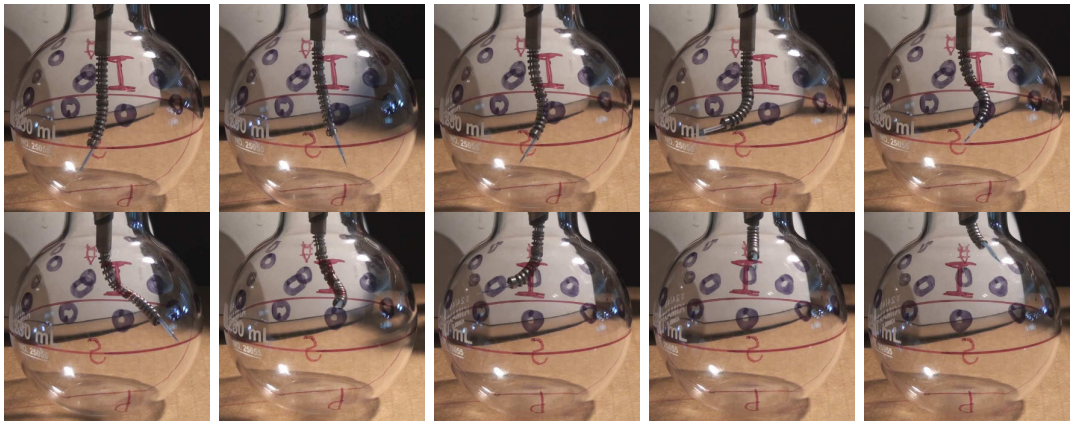

Fig. 7. Picture sequence of bladder coverage. The slave manipulator, under telemanipulation control, is guided to cover progressively the posterior and interior quadrants. The manipulator goes from a completely deployed configuration to a completely folded configuration into the urologic resectoscope.

## REFERENCES


[1] R. J. Webster III and B. A. Jones, "Design and Kinematic Modeling of Constant Curvature Continuum Robots: A Review," *The Int. J. of Robotics Research*, pp. 1661–1683, Jun. 2010.

[2] N. Simaan, K. Xu, W. Wei, A. Kapoor, P. Kazanzides, R. H. Taylor, and P. Flint, "Design and Integration of a Telerobotic System for Minimally Invasive Surgery of the Throat," *The International Journal of Robotics Research*, vol. 28, no. 9, pp. 1134–1153, 2009.

[3] C. Bedell, J. Lock, A. Gosline, and P. E. Dupont, "Design Optimization of Concentric Tube Robots Based on Task and Anatomical Constraints." *2011 IEEE Int. Conf. on Robotics and Automation*, pp. 398–403, 2011.

[4] S. B. Kesner, R. D. Howe, and S. Member, "Position Control of Motion Compensation Cardiac Catheters," *IEEE Transaction on Robotics*, vol. 27, no. 6, pp. 1045–1055, 2011.

[5] J. Burgner, P. J. Swaney, D. C. Rucker, H. B. Gilbert, S. T. Nill, P. T. Russell, K. D. Weaver, and R. J. Webster, "A bimanual teleoperated system for endonasal skull base surgery," in *2011 IEEE/RSJ Int. Conf. on Int. Robots and Systems*, 2011, pp. 2517–2523.

[6] R. E. Goldman, A. Bajo, L. K. Suh, R. B. Pickens, S. D. Herrell, and N. Simaan, "Design and Evaluation of a Minimally Invasive Telerobotic Platform for Transurethral Intervention and Surveillance," *IEEE Trans. on Biomedical Engineering*, vol. accepted, 2013.

[7] G. S. Chirikjian and J. W. Burdick, "An obstacle avoidance algorithm for hyper-redundant manipulators," in *1990 IEEE Int. Conf. on Robotics and Automation*, 1990, pp. 625–631.

[8] S. Ma and M. Konno, "An obstacle avoidance scheme for hyper-redundant manipulators-global motion planning in posture space," in *Proc. of Int. Conf. on Robotics and Automation*, vol. 1, no. April. IEEE, 1997, pp. 161–166.

[9] "Suturing in Confined Spaces: Constrained Motion Control of a Hybrid 8-DoF Robot"," in *IEEE Conf. on Advanced Robotics*, 2005, pp. 452–459.

[10] A. Kapoor and R. H. Taylor, "A Constrained Optimization Approach to Virtual Fixtures for Multi-Handed Tasks," in *2008 IEEE Int. Conf. on Robotics and Automation*, Pasadena, CA, 2008, pp. 3401–3406.

[11] L. G. Torres and R. Alterovitz, "Motion Planning for Concentric Tube Robots Using Mechanics-based Models," in *2011 IEEE/RSJ Int. Conf. on Intelligent Robots and Systems*, San Francisco, CA, USA, 2011, pp. 5153–5159.

[12] E. Sanchez de Badajoz, A. Jimenez-Garrido, V. F. Munoz Martinez, J. M. Gomez de Gabriel, and A. Garcia Cerezo, "New Master Arm for transurethral resection with a robot [Article in Spanish]," *Archivos espanoles de urologia*, vol. 55, no. 10, pp. 1247–50, 2002.

[13] M. Aron and M. M. Desai, "Flexible Robotics," *The Urologic Clinics of North America*, vol. 36, no. 2, pp. 157–62, 2009.

[14] R. Hashimoto, D. Kim, N. Hata, T. Dohi, and A. S. Requiremerir, "A Tubular Organ Resection Manipulator for Transurethral Resection of the Prostate," in *2004 IEEE Int. Conf. on Int. Robotis and Systems*, Sendai, Japan, 2004, pp. 3954–3959.

[15] W. J. Yoon, S. Park, P. G. Reinhall, and E. J. Seibel, "Development of an Automated Steering Mechanism for Bladder Urothelium Surveillance," *Journal of Medical Devices*, vol. 3, no. 1, p. 011004, 2009.

[16] D. Kragic, P. Marayong, Li-Ming Su, A. M. Okamura, and G. D. Hager, "Human-Machine Collaborative Systems for Microsurgical Applications," *The Int. J. of Robotics Research*, vol. 24, no. 9, pp. 731–741, Sep. 2005.

[17] NIH, "National Cancer Institute," 2012. [Online]. Available: http://www.cancer.gov/cancertopics/types/bladder

[18] K. Xu and N. Simaan, "Analytic Formulation for Kinematics, Statics, and Shape Restoration of Multibackbone Continuum Robots Via Elliptic Integrals," *ASME Journal of Mechanisms and Robotics*, vol. 2, no. 1, 2010.

[19] ——, "An Investigation of the Intrinsic Force Sensing Capabilities of Continuum Robots," *IEEE Transactions on Robotics*, vol. 24, no. 3, pp. 576–587, Jun. 2008.

[20] A. Bajo, R. E. Goldman, L. Wang, D. Fowler, and N. Simaan, "Integration and preliminary evaluation of an Insertable Robotic Effectors Platform for Single Port Access Surgery," in *2012 IEEE Int. Conf. on Robotics and Automation*, St. Paul, MN USA, 2012, pp. 3381–3387.

[21] D. E. Whitney, "Resolved Motion Rate Control of Manipulators and Human Prostheses," *IEEE Transaction on Man-Machine Systems*, vol. MMS-10, no. 2, pp. 47–53, 1969.

[22] K. Xu and N. Simaan, "Actuation Compensation for Flexible Surgical Snake-like Robots with Redundant Remote Actuation," in *2006 IEEE Int. Conf. on Robotics and Automation*, no. May, Orlando, FL, 2006, pp. 4148–4154.